8 NMR Characterization of Emulsions

Alejandro A. Peña and George J. Hirasaki

CONTENTS

8.1 INTRODUCTION

Emulsions are among man-made commodities such as food goods [1,2], cosmetics [3,4], paints [5], agricultural sprays [6,7], asphalt preparations [8], and pharmaceuticals [4,7]. Emulsions are also found as undesired byproducts of industrial processes, including crude oil production [9,10] and liquid–liquid extraction operations [11]. Information on the microstructure and composition of an emulsion is relevant whether its making is sought or unwanted, because such information can be related to important properties of the dispersion such as its viscosity [12–14] and its stability against phase separation [15,16], and also to quality control standards. For example, the color [17] and texture (creaminess) [18] of food emulsions are known to depend on the distribution of droplet sizes; crude oil streams with emulsified water content in excess of a given threshold are not suited for processing in refining equipment [19].

Experimental techniques such as microphotography and video-enhanced microscopy, gravitational/centrifugal sedimentation, Coulter counting, differential scanning calorimetry, turbidimetry, dynamic and static light scattering, low-intensity ultrasound, and nuclear magnetic resonance (NMR) have been used to characterize emulsions [20–22]. NMR-based techniques are becoming increasingly popular due to practical advantages that they offer over other above-mentioned techniques. For example, the same emulsion sample can be tested via NMR as many times as desired. Dilution, cooling/heating, centrifugation, or confinement in a narrow gap are not necessary. Measurements are not influenced by the optical or dielectric properties of the system. Therefore, clear and opaque emulsions, and dispersions in which the continuous phase is nonconducting, can be tested. A typical NMR test is fast ($\sim$ 1 to 10 min), and it requires a small sample ($\geq\sim$ 0.5 g). Furthermore, the composition of the emulsion can be resolved from the NMR data.

Important progresses have been made in the characterization of emulsions via NMR since the publication of the first edition of this book in 1996. Efforts in recent years have been mainly focused on (1) expanding the theory and techniques used to interpret self-diffusion data obtained from the classic pulsed field gradient (PGSE) experiments for the determination of the microstructure and stability of emulsions, to overcome limitations that were inherent to classic views; (2) use alternative NMR pulsed sequences to allow data acquisition in shorter timescales, both for quiescent and flowing emulsions; and (3) utilize NMR-based techniques in applications involving the usage of emulsions, and for which such methods had not been previously considered. This chapter provides a critical compendium of such progress. The discussion is developed while presenting a brief introduction of NMR principles and techniques that are relevant to emulsion characterization.

8.2 BASIC NMR PRINCIPLES

NMR microscopy on emulsions is based on the following few physical principles [23]: Some nuclei, such as protons (^{1}H), exhibit a magnetic moment μ. When a steady uniform magnetic field $\mathbf{B_0}$ is applied on these nuclei, μ precesses around the direction of $\mathbf{B_0}$ at the Larmor frequency $\omega_0 = \gamma B_0$, where γ is a constant. Nuclei with precessing μ are termed *spins*. The ensemble of spins exhibits net magnetization $\mathbf{M}$ in the direction of $\mathbf{B_0}$. If a *radio frequency* (*rf*) *pulse* of a second magnetic field $\mathbf{B_1}$ orthogonal to $\mathbf{B_0}$ is applied, the net magnetization is rotated to an extent (typically 90° or 180°) that depends on the duration of the pulse. When the rf pulse ceases, $\mathbf{M}$ will *relax* toward and eventually reach some equilibrium state. Relaxation of $\mathbf{M}$ can be measured from the spins present in the emulsion, either in the direction of $\mathbf{B_0}$ (longitudinal magnetization), or transverse to it (transverse magnetization), whence characteristic relaxation rates can be quantified in terms of specific sets of longitudinal (T_1) and transverse (T_2) relaxation times, respectively.

In addition, the precession of spins at the same frequency is referred to as coherent or in-phase. If the steady magnetic field is not uniform as above the frequency depends on the position of the nuclei [$\omega(\mathbf{r}) = \gamma \mathrm{B}(\mathbf{r})$]. Two spins at positions $\mathbf{r_a}$ and $\mathbf{r_b}$, such that $\mathbf{B}(\mathbf{r_a}) \neq \mathbf{B}(\mathbf{r_b})$, precess incoherently out of phase. Magnetic field gradients are commonly applied to create a non-uniform steady magnetic field and adjust coherence.

Structural information of the emulsion, such as droplet sizes, relative concentration of the immiscible phases present, and morphology (water-in-oil, W/O vs. oil-in-water, O/W), can be inferred from the time-resolved signal as discussed later. Furthermore, Fourier transformation of the signal renders the NMR spectrum of the sample, whence individual chemical components can be identified and their concentrations determined [24–26]. Low-frequency NMR spectrometers

operating at 2 to 20 MHz suffice for time-resolved signal applications and are most commonly used in industrial applications. High-frequency (typically 400 to 800 MHz) NMR spectrometers are required to obtain NMR spectra with adequate resolution for detailed spectroscopic applications.

Whereas most NMR experiments on emulsions rely on measurements on ^{1}H nuclei due to their natural abundance, spectroscopic studies on emulsions targeting ^{19}F [27,28], ^{31}P [29–34], ^{13}C [34], and ^{129}Xe [35,36] nuclei have also been reported, as described in recent reviews on this subject [37,38]. For the sake of brevity, the descriptions of basic NMR pulsed sequences given in Sections 8.3 and 8.4 are supplemented with data from ^{1}H studies. The reader should keep in mind, however, that such sequences can be applied, in principle, to fluids containing other nuclei such as those listed above.

8.3 RELAXATION MEASUREMENTS ON EMULSIONS VIA CPMG EXPERIMENTS

8.3.1 The CPMG Pulsed Sequence

The CPMG pulsed sequence bears the initials of its developers, Carr and Purcell [39], who first introduced it, and Meiboom and Gill [40], who further refined it to make it suitable for routine experiments. It consists of a rf 90° pulse, followed by N rf 180° pulses that induce successive phase recoveries and generate a train of N spin-echoes (Figure 8.1). As time proceeds, relaxation of the magnetization occurs and the amplitude of the spin-echo that is generated after each 180° re-phasing decays. In this experiment, the transverse component of the magnetization vector $M_{xy}(2n\tau)$ is measured, and the resulting relaxation curve is fitted to a discrete multi-exponential function of the form:

$$\frac{M_{xy}(2n\tau)}{M_{xy}(0)} = \sum_{i=1}^{m} f_i \exp\left(-\frac{2n\tau}{T_{2,i}}\right); \quad 0 \le n \le N; \quad m < N; \quad \sum_{i=1}^{m} f_i = 1 \tag{8.1}$$

$M_{xy}(0)$ is the amplitude of signal that corresponds to the initial transverse magnetization and f_i is the fraction of nuclei with characteristic relaxation time $T_{2,i}$. The fitting procedure consists of calculating f_i values for a pre-established set of $T_{2,i}$, whence the T_2 distribution is obtained. Fitting data to a multi-exponential sum is an ill-posed problem, i.e., multiple sets of f_i values can render a satisfactory fit [41]. For this reason, a regularization method must be implemented to calculate the most representative T_2 distribution [42].

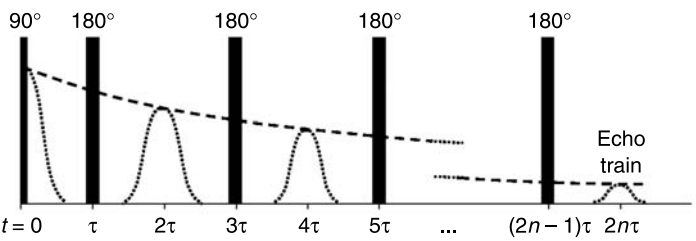

FIGURE 8.1 Sequence of events in a CPMG experiment.

8.3.2 Determination of the Water/Oil Composition in Emulsions via CPMG

In a CPMG test, the amplitude of the signal that is obtained for a given sample is proportional to the number of spins present in such sample. This principle allows relating the water/oil ratio of common O/W and W/O emulsions to the T_2 distribution obtained from ^{1}H CPMG experiments through the expression:

$$\frac{\phi_W}{\phi_O} = \frac{\sum(f_i)_W/HI_W}{\sum(f_i)_O/HI_O} \tag{8.2}$$

whence

$$\phi_W = \frac{\left[\sum(f_i)_W/HI_W\right]}{\left[\sum(f_i)_W/HI_W\right] + \left[\sum(f_i)_O/HI_O\right]}; \quad \phi_O = 1 - \phi_W \tag{8.3}$$

ϕ_k is the volume fraction of phase k present in the emulsion. *HI* is the hydrogen index, which is defined as the number of protons in a sample divided by the number of protons present in the same volume of water [43]. The calculation of *HI* for pure fluids using this definition is straightforward. Empirical correlations and diagrams to estimate *HI* are available for "water" phases such as brines and "oil" phases such as light and heavy crude oils [44–46]. In general, $HI \sim 1.0$ for aqueous solutions and $HI \sim 0.9$ to 1.0 for most crude oils except for aromatic oils, which exhibit *HI* between 0.6 and 0.8 due to the low H/C ratio of aromatic compounds.

Figure 8.2 summarizes results from ^{1}H CPMG experiments performed with a 2-MHz spectrometer on thirty water-in-crude oil emulsions prepared at different water/oil compositions and containing the same crude oil ($HI = 0.928$) [47]. Figure 8.2(a) shows the T_2 distributions that were obtained for six of these samples, normalized with respect to the oil signal. It is seen in Figure 8.2(a) that the signal from the water phase increases with the water content, as might be expected. Figure 8.2(b) compares the actual water content of these and other mixtures with the water content that is calculated using Equation 8.3. The excellent agreement that was found between actual and measured water contents illustrates the usefulness of the technique to resolve for the water/oil composition of emulsions.

Low-field NMR-CPMG has been regarded as superior to all other available techniques for the routine determination of water content in heavy oil, bitumen, and oilfield emulsions [48,49]. This application of the CPMG method has been discussed by LaTorraca et al. [43] and Hills et al. [50]. Allsopp et al. [48] have developed and successfully tested *in situ* a low-field spectrometer suitable for usage in the field. The method was accurate to ± 5% and measuring times were typically 4 min or less. This application is a natural extension of the usage of NMR relaxation measurements for the determination of porosity in minerals and rocks [51–54].

8.3.3 Determination of Drop Sizes and Stability of Emulsions via CPMG

Equation 8.1 arises naturally when the relaxation of magnetization is modeled for an isotropic fluid confined in a planar, cylindrical, or spherical cavity in the presence of volume-like and surface-like magnetization sinks with average constant strength $1/T_{2,bulk}$ (*bulk relaxivity*) and ρ (*surface relaxivity*), respectively [55]. The contributions of bulk and surface relaxivity to the decay of transverse magnetization are accounted for in the $T_{2,i}$ values as follows:

$$\frac{1}{T_{2,i}} = \frac{1}{T_{2,bulk}} + \rho\left(\frac{S}{V}\right)_i \tag{8.4}$$

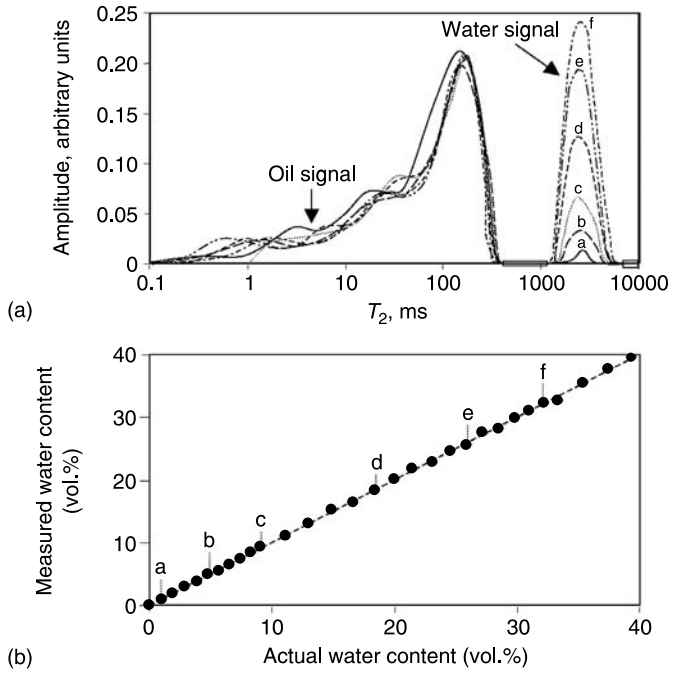

FIGURE 8.2 Determination of the water/oil composition of emulsions via low-field NMR CPMG experiments. (a) The signal from the water phase increases with water content. (b) Comparison of actual water content with that measured by using Equation 8.3.

$(S/V)_i$ is the surface-to-volume ratio of the cavity i. For a sphere of radius a_i, $(S/V)_i = 3/a_i$. Hence,

$$\frac{1}{T_{2,i}} = \frac{1}{T_{2,bulk}} + \rho\frac{3}{a_i} \tag{8.5}$$

and

$$a_i = 3\rho\left(\frac{1}{T_{2,i}} - \frac{1}{T_{2,bulk}}\right)^{-1} \tag{8.6}$$

Equations 8.4 to 8.6 are valid in the fast diffusion limit, in which the characteristic timescale for diffusion of the molecules confined in the drops (t_D) is much smaller than the characteristic timescale for surface relaxation (t_ρ):

$$\frac{t_D}{t_\rho} = \frac{a_i^2/D}{a_i/\rho} \ll 1, \text{ whence } \frac{\rho a_i}{D} \ll 1 \tag{8.7}$$

D is the self-diffusion coefficient of the drop phase. In practice, the relaxation of magnetization of fluids confined in spherical cavities occurs in the fast diffusion mode whenever $\rho a/D <\sim 0.25$.

It was shown that the number of protons present in a given volume of sample determines the signal amplitude. For this reason, the fraction f_i that is associated to each $T_{2,i}$ value renders a direct measurement of the fraction of fluid that is confined in cavities of corresponding surface-to-volume ratio $(S/V)_i$. Therefore, the T_2 distribution that is obtained from isotropic fluids contained in the interstices of a heterogeneous system contains valuable information on the distribution of sizes of such heterogeneities. Equation 8.6 can thus be used to calculate the volume-weighted drop size distribution of emulsions containing spherical droplets, provided that:

1. Two independent sets of $T_{2,i} - f_i$ values can be resolved from the T_2 distribution of the emulsion for the oil and water phases, respectively. This task is straightforward if the water signal and oil signal appear as separate peaks in the T_2 distribution, such as those shown in Figure 8.2. Otherwise, methods such as the diffusion-editing CPMG (DE-CPMG) [56] or the magnetic resonance fluid method [57] can be used to discriminate water signal from oil signal for systems in which the T_2 distributions of these phases overlap.
2. The surface relaxivity (ρ) and the bulk relaxivity ($1/T_{2,bulk}$) of the drop phase (water in *w/o* emulsions or vice versa) are known. $T_{2,bulk}$ can be easily measured from a CPMG experiment on a bulk sample of the drop phase, either in absence of continuous phase or in contact with it, but not emulsified. An independent measurement of the surface-to-volume ratio of the emulsion is required to calculate ρ as discussed later.

Figure 8.3(a) shows (solid line) the T_2 distribution of an emulsion containing 30 vol% water in crude oil. Details on the preparation of samples and test conditions are given in Ref. 47. The T_2 distribution of the water and oil phases were also measured from individual samples of each phase (dotted lines). The most significant feature of Figure 8.3(a) is the fact that the signal of the water phase present in the emulsion shifted towards lower relaxation times. Such shift is caused by relaxation of the magnetization at the water–oil interfaces that are created once the water phase was dispersed as droplets within the oil phase. Figure 8.3(b) shows a comparison of NMR-CPMG measurements with microphotography measurement for the same emulsion. The NMR data were calculated by replacing the T_2 data for the water phase of the emulsion shown in Figure 8.3(a) in Equation 8.6 using a surface relaxivity of 0.88 μm/s, which was determined concomitantly with data acquired using the NMR-PGSE method as described in Section 8.4. For the particular tests shown here, it is seen that the CPMG method adequately describes both the numerical values for drop sizes and also the distribution of such sizes. An important feature of the NMR-CPMG method shown in Figure 8.3 is that it allows the resolution for drop size distributions with arbitrary shape, i.e., it does not require assuming a priori a mathematical expression such as the log–normal distribution that is commonly used to interpret drop size distribution measurements using the NMR-PGSE technique [26,58–65].

It has been proposed [47] that the minimum and maximum drop sizes that can be determined via CPMG are, respectively:

$$d_{MIN} \cong 6\rho T_{2,\min} \tag{8.8}$$

and

$$d_{MAX} \cong \min\{D/2\rho, 2e^{-1}SNR\rho T_{2,bulk}\} \tag{8.9}$$

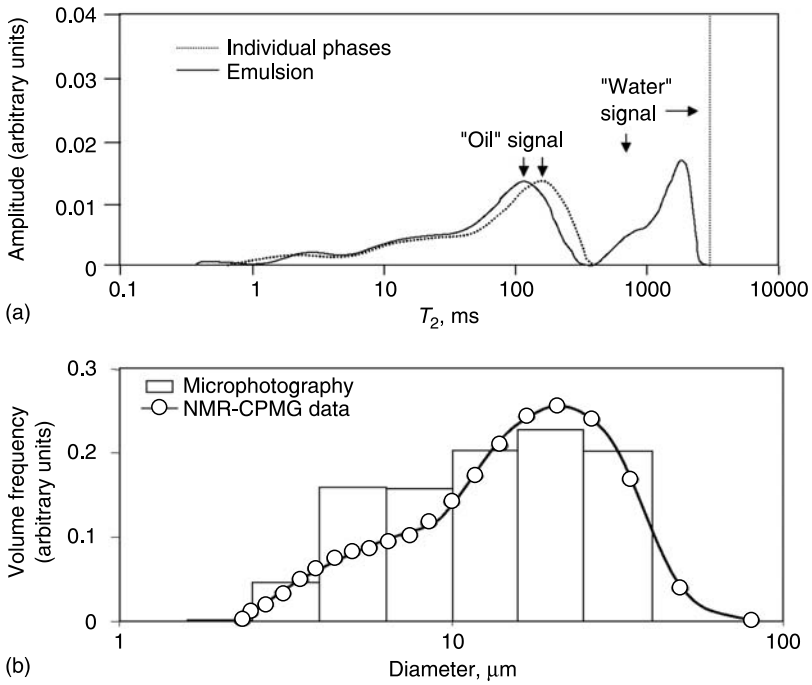

FIGURE 8.3 (a) T_2 distribution of a water-in-crude oil emulsion (W/O ratio = 30/70 (vol.)); (b) calculated drop size distribution from the T_2 distribution of the water phase, using $\rho = 0.88$ μm/s.

where *SNR* is the signal-to-noise ratio ($SNR = M_{xy}(t = 0)/v$, with v being the intrinsic noise of the measurement) and $T_{2,\min} = -2\tau/\ln(1 - \varepsilon)$, where ε is the fraction of the transverse component of magnetization of the fluid present in drops with diameter d_{MIN} that has relaxed when the first echo is acquired at time 2τ (Figure 8.1), i.e., the fraction of droplets with $d = d_{MIN}$ that would not be accounted for due to relaxation before the acquisition of the first spin-echo. The expression for d_{MIN} is valid whenever $T_{2,\min} \ll T_{2,bulk}$. Using the data reported in Ref. 47 ($D = 2.3 \times 10^{-9}$ m^2/s, $SNR = 99.7\%/0.3\% = 332$, $T_{2,bulk} = 2.8$ s, $2\tau = 315$ ms) with $\rho = 0.88$ μm/s and $\varepsilon = 0.1$, Equations 8.8 and 8.9 render $d_{MIN} = 16$ nm and $d_{MAX} = 580$ μm. These figures illustrate that, in principle, a very wide range of droplet sizes can be measured using the CPMG technique. In many practical cases, however, the minimum drop size may be limited by the ability to distinguish the water from the oil signal if they overlap.

The NMR-CPMG experiment is also useful for performing drop size distribution measurements in emulsions with limited stability. Figure 8.4 shows NMR-CPMG transient drop size distribution data for two emulsions of 5 wt% NaCl brine (30 vol%) in crude oil (70 vol%) that were treated with chemicals commonly used in demulsification operations [66]. Results shown in Figure 8.4(a) correspond to an emulsion sample treated with a nonylphenol formaldehyde resin. Results given in Figure 8.4(b) correspond to a sample of the same emulsion treated with a polyurethane. The data shown in Figure 8.4 depict a fast and steady growth of drop sizes, thus indicating that the nonylphenol formaldehyde resin induced rapid coalescence. In contrast, Figure 8.4(b) illustrates the inability of the polyurethane used in the experiment to induce significant coalescence. A shortcoming of this procedure is the fact that the surface relaxation

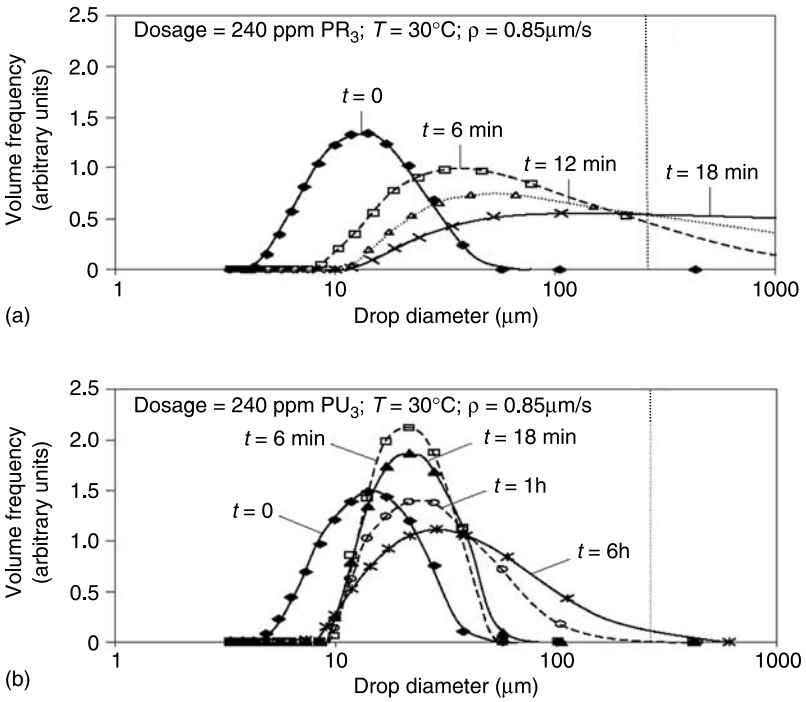

FIGURE 8.4 Drop size distributions of water-in-crude oil emulsions (W/O ratio = 30/70 (vol.)) undergoing phase separation as measured via NMR-CPMG: (a) emulsion treated with a nonylphenol formaldehyde resin (PR); (b) emulsion treated with a polyurethane (PU). Details on the experiment are given in Ref. 66.

is assumed constant throughout the phase separation process. Whereas the validity of such an assumption deserves consideration in future studies, the result is still useful because it provides a reference for the timeframes for which significant changes in the microstructure of the emulsion occur.

An interesting extension of the NMR-CMPG method consists of applying the sequence shown in Figure 8.1 in the presence of a magnetic field gradient (CPMG gradient or CPMG-g test). When a gradient of strength g is imposed, the steady magnetic field is not uniform in space and the Larmor frequency depends on the position of the nuclei [$\omega(\mathbf{r}) = \gamma \mathrm{B}(\mathbf{r})$] as mentioned earlier. The coil ("antenna") of the spectrometer is tuned to measure the response of the region where spins precess at a specific Larmor frequency ω_0. Therefore, only those spins are sensed by the spectrometer. This principle allows characterizing "slices" of the sample of interest. In this case, an additional contribution to the relaxation time T_2 is caused by the diffusion of the spins in the field gradient and Equation 8.5 becomes:

$$\frac{1}{T_{2,i}} = \frac{1}{T_{2,bulk}} + \rho\frac{3}{a_i} + \frac{(\gamma g t_E)^2 D}{12} \tag{8.10}$$

where $t_E = 2\tau$ is the time between consecutive 180° rf pulses (Figure 8.1) and γ is a physical constant called the gyromagnetic ratio that has a specific value for each nuclei ($\gamma = 2.67 \times 10^8$ rad $\mathrm{T}^{-1}\mathrm{s}^{-1}$ for $^1\mathrm{H}$).

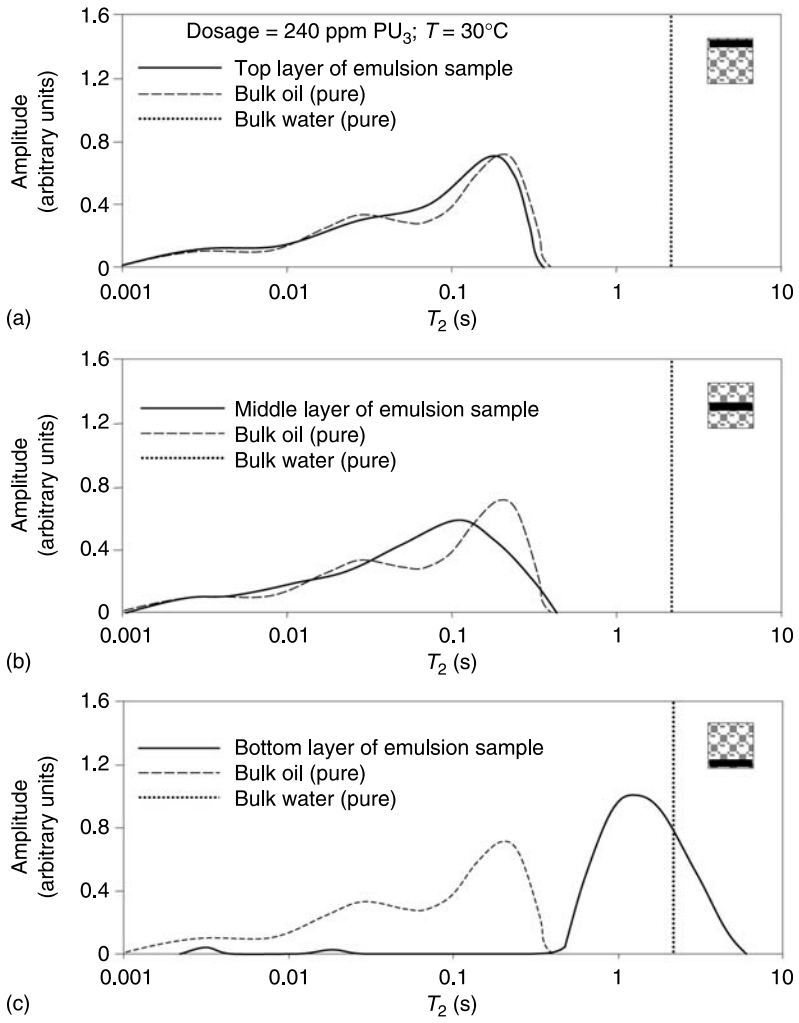

FIGURE 8.5 T_2 distributions of selected regions of the emulsion treated with a polyurethane. Data were obtained using the CMPG-*g* pulsed sequence.

Figure 8.5 shows the T_2 distributions that were obtained after applying the CPMG-*g* method on three regions (top, middle, and bottom) of the sample treated with the polyurethane for which data were reported in Figure 8.4(b). The T_2 distributions of the crude oil (dashed line) and of the brine (dotted line) are also shown as reference. Details on the experiment are provided in Ref. 66, the most important being that a clear layer of decanted water could not be observed at the bottom of the sample at the time that the experiment was performed. Nevertheless, the comparison of the T_2 distributions for "slices" of the emulsion with those of the individual phases clearly shows that the upper and middle regions of the sample had been deprived of water, which otherwise had accumulated at the bottom. These data, along with bottle tests and viscosity measurements, suggest that the polyurethane that was used in the experiment depicted in Figures 8.4(b) and 8.5 was able to induce flocculation and rapid sedimentation of

the water droplets, but without causing significant coalescence. The ability to evaluate details of the microstructure in specific regions of opaque emulsions without having to destroy the sample (or aliquots of it) is a feature of NMR-based techniques that cannot be procured by any other experimental method.

8.3.4 Advantages and Limitations of the CPMG Experiment

Perhaps the most advantageous feature of the CPMG method is that thousands of spin-echoes are acquired in one test (typically over 10,000). From the large dataset that is obtained in this experiment, drop size distributions with arbitrary shape can be determined. The calculations reported above suggest that the method can resolve drop sizes ranging from $\sim$ 0.01 to $\sim$ 500 microns. In addition, the water/oil composition of the emulsion can be calculated. A CPMG test typically takes about five minutes to be completed. The short duration of the test makes it suitable to keep track of the stability of the emulsion and of rapid changes in the drop size distribution. Finally, the CPMG test is independent of the self-diffusivity of the phases because it is performed in absence of magnetic field gradients. Therefore, the T_2 distribution of the emulsion can be fully interpreted in terms of natural (bulk) and surface relaxation. When magnetic field gradients are used (CMPG-g test), it is feasible to obtain structural information of selected regions of the sample without perturbing it. On the other hand, the surface relaxivity cannot be determined from CPMG alone. An independent measurement of the surface-to-volume ratio is required to evaluate ρ.

8.4 DIFFUSION MEASUREMENTS ON EMULSIONS VIA PGSE AND PGSTE EXPERIMENTS

8.4.1 The PGSE Pulsed Sequence

In 1965, Tanner and Stejskal [67] first reported an attempt to correlate NMR data with drop sizes in emulsions via the pulsed magnetic field gradient spin-echo experiment (PGSE), which had been published by them a few years before [68]. The basic PGSE pulsed sequence consists of a rf 90° pulse, followed by a rf 180° pulse at time τ (Figure 8.6(a)). As a result of this sequence, a spin-echo is collected at time 2τ. The rf 180° pulse is sandwiched between two magnetic field gradient pulses of absolute strength g and duration δ that are separated by a time span Δ.

In a PGSE experiment, the amplitudes of the spin-echoes in the presence and absence of gradient pulses ($g > 0$ and $g = 0$, respectively) are measured. In the latter case, the spin-echo is acquired in a homogeneous magnetic field and therefore $M_{xy}(2\tau,\ g = 0,\ \Delta,\ \delta)$ is independent of the spatial distribution of spins in the sample. On the other hand, when $g > 0$ the first gradient pulse imposes an inhomogeneous magnetic field, thus causing a loss of coherence in the phases of the spins to an extent that depends on the position of the nuclei at the time the gradient is applied. In the absence of diffusion, the second gradient pulse would exactly reverse the phase shifts. However, since molecules diffuse and change their position during the *diffusion time* Δ, the refocusing is incomplete and the amplitude of the echo that is recorded at time 2τ [$M_{xy}(2\tau,\ g > 0,\ \Delta,\ \delta,\ D)$] is smaller than $M_{xy}(2\tau,\ g = 0,\ \Delta,\ \delta)$. For this reason, $0 < M_{xy}(2\tau,\ g,\ \Delta,\ \delta,\ D) < M_{xy}(2\tau,\ g = 0,\ \Delta,\ \delta)$. Whence,

$$R = \frac{M_{xy}(2\tau, g, \Delta, \delta, D)}{M_{xy}(2\tau, g = 0, \Delta, \delta)}; \quad 0 \le R \le 1 \tag{8.11}$$

R is termed the *spin-echo attenuation ratio*. In a typical PGSE experiment, attenuation ratios are measured changing systematically δ, Δ, or g.

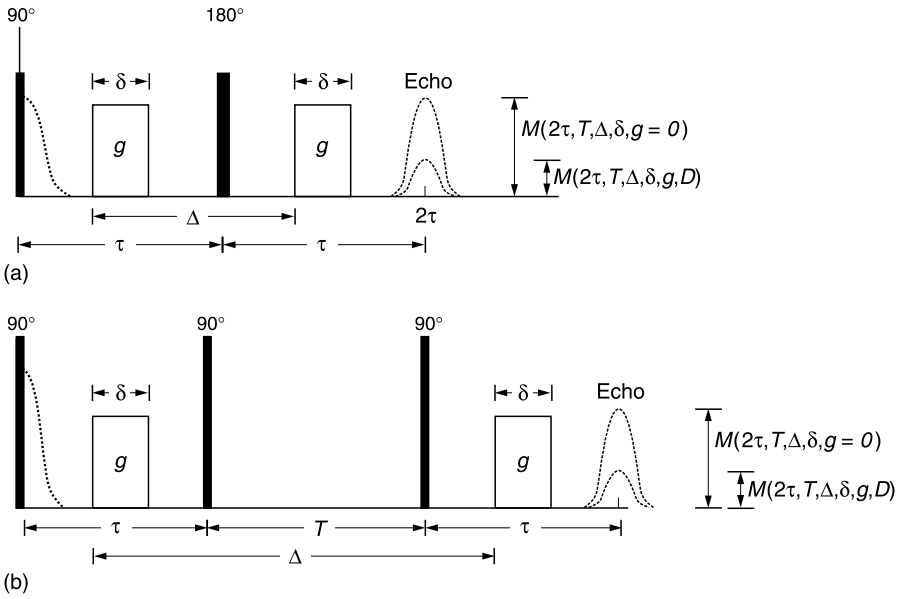

FIGURE 8.6 Basic (a) PGSE and (b) PGSTE pulsed sequences.

8.4.2 The PGSTE Pulsed Sequence

The stimulated spin-echo pulsed field gradient (PGSTE), which was also introduced by Tanner [69] (Figure 8.6(b)), is particularly useful for systems exhibiting significantly different longitudinal (T_1) and transverse (T_2) relaxation times ($T_1 > T_2$). This is often the case for systems exhibiting a large interfacial area, such as emulsions. By virtue of the second rf 90° pulse, the direction of the magnetization vector is shifted in a way that its initially transverse (xy) component is positioned in the longitudinal (z) direction, upon which relaxation of magnetization occurs at a slower rate (characteristic relaxation rate $= 1/T_1 < 1/T_2$). The third rf 90° pulse repositions M_{xy} in the transverse plane. As a result, a "stimulated" spin-echo occurs an interval after the third rf pulse equal to that between the first two pulses. This procedure allows increasing the diffusion time Δ while reducing the deleterious effect of extended relaxation upon the signal-to-noise ratio that otherwise would occur when increasing Δ for the 90° to 180° PGSE pulsed sequence. This feature has made the PGSTE sequence the NMR pulsed sequence of choice for a large number of experimental studies on emulsions (see, for example, Refs. 70–76). The definition for the attenuation ratio R given by Equation 8.11 also applies to PGSTE tests, with the acquisition time being $2\tau + T$ instead of 2τ. The mathematical description that follows is valid both for PGSE and PGSTE experiments, unless otherwise indicated.

8.4.3 Determination of Drop Sizes in Emulsions via PGSE and PGSTE

For isotropic bulk fluids in which molecules can diffuse freely (Fickian diffusion), the following expression holds [68]:

$$R_{bulk} = \exp\left[-\gamma^2 g^2 D\delta^2\left(\Delta - \frac{\delta}{3}\right)\right] \tag{8.12}$$

When Equation 8.12 holds, a plot of the logarithm of R vs. $g^2\ \delta^2(\Delta - \delta/3)$ renders a straight line, and D can be calculated from the slope. This method is one of the very few experimental techniques available to measure self-diffusion coefficients.

Equation 8.12 does not apply to fluids confined in small geometries such as pores or droplets, because molecules cannot diffuse freely. In this case, the dimensions of the cavity limit the distance the spins diffuse by Brownian motion, thus affecting the attenuation ratio R. Robertson [77] and Neuman [78] first proposed expressions for R for molecules confined between planes and within cylinders and spheres when a steady magnetic field gradient is applied. Murday and Cotts [79] extended Neuman's derivation for the PGSE sequence for restricted diffusion within a sphere of radius a. In this case, the attenuation ratio R_{sp} was shown to be given by:

$$R_{sp} = \exp\left\{-2\gamma^2 g^2 \sum_{m=1}^{\infty} \frac{1}{\alpha_m^2(\alpha_m^2 a^2 - 2)}\left[\frac{2\delta}{\alpha_m^2 D} - \frac{\Psi}{(\alpha_m^2 D)^2}\right]\right\} \tag{8.13}$$

where

$$\Psi = 2 + \exp\lfloor -\alpha_m^2 D(\Delta - \delta)\rfloor - 2\exp(-\alpha_m^2 D\Delta) - 2\exp(-\alpha_m^2 D\delta) + \exp\lfloor -\alpha_m^2 D(\Delta + \delta)\rfloor \tag{8.14}$$

α_m is the m^{th} positive root of the equation:

$$\alpha a \cdot J_{5/2}(\alpha a) - J_{3/2}(\alpha a) = 0 \tag{8.15}$$

and J_k is the Bessel function of the first kind, order k. Figure 8.7 shows theoretical calculations for R using Equations 8.13 to 8.15 (solid lines) for selected values of a. It is seen that the attenuation of R is less for smaller cavities.

Two limiting cases of Equation 8.13 are of interest. First, for very large spheres ($a \to \infty$), Equation 8.13 reduces to Equation 8.12 [$R_{sp}(a \to \infty) = R_{bulk}$]. Calculations for the attenuation ratio using Equation 8.12 are also reported in Figure 8.7 (squares) to show the agreement of this expression with Equation 8.13 for large values of a.

Second, for very small spheres, Equation 8.13 simplifies as follows:

$$R_{sp} = 1 - \frac{16}{175}\gamma^2 g^2 D^{-1}\delta a^4 \tag{8.16}$$

whence $R_{sp}(a \to 0) = 1$. In this case, the probability of the molecules to displace during the diffusion time Δ is reduced as $a \to 0$. For this reason, the loss of coherence in the phases of the spins caused by the magnetic field gradient diminishes and less attenuation of the spin-echo is observed. Figure 8.7 (inserted plot) also illustrates the agreement between Equation 8.16 (circles) and Equation 8.13 (solid lines) for small spheres.

In the derivation of Equation 8.13 it is assumed that the phase shifts of spins diffusing in a bounded region exhibit a normal (Gaussian) distribution. However, this Gaussian phase-distribution (GPD) approximation is exact only for spins undergoing free diffusion [78]. Balinov et al. [80] performed Brownian dynamic simulations for restricted diffusion in spheres of selected sizes at fixed g, Δ, and for various δ to calculate the *exact* attenuation ratio that would be observed in each case. Least-squares fits of these results were performed using Equation 8.13 and the sphere radius a as fitting parameter. The radii calculated with this expression differed by less than 5%

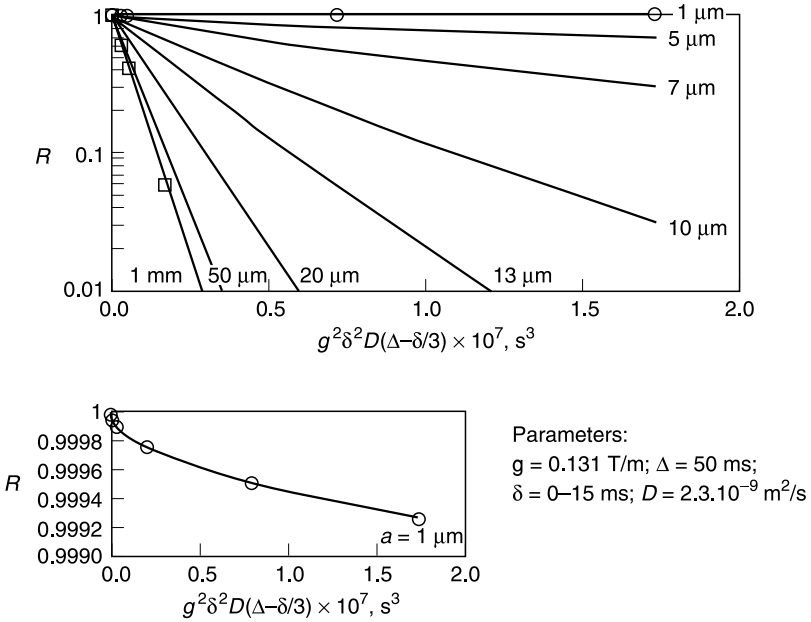

FIGURE 8.7 Theoretical calculations for the PFG attenuation ratio using Equation 8.13 (solid lines) and the limiting expressions for large values of a (Equation 8.12, squares) and for small values of a (Equation 8.16, circles; see also inserted plot for $a = 1$ μm).

from the sizes set for the simulations. Whence it was concluded that the GPD approximation and Equation 8.13 are adequate to account for the decay of transverse magnetization of fluids confined in spheres.

For emulsion with a finite distribution of (spherical) droplet sizes, Packer and Rees [58] first proposed that the attenuation ratio of the drop phase (R_{DP}) can be calculated as the sum of the attenuation ratios $R_{sp}(a)$ that would be recorded for fluid confined in drops of radii a, weighted by the probability of finding drops with such sizes in the dispersion. This is:

$$R_{DP} = \int_0^\infty p_V(a) R_{sp}(a) da \Big/ \int_0^\infty p_V(a) da \tag{8.17}$$

where $p_V(a)$ is the volume-weighted distribution of sizes, and $R_{sp}(a)$ is given by Equation 8.13. The task of determining $p_V(a)$ from the PGSE data is feasible, but requires a large number of measurements of R for which the duration of the test may become impractical as discussed later. Instead, few data are usually taken and an empirical form of $p_V(a)$ is assumed. The log–normal probability distribution function (p.d.f.),

$$p_V(a) = \frac{1}{2a\sigma(2\pi)^{1/2}} \exp\left\{-\left[\frac{\ln(2a) - \ln(d_{gV})}{2\sigma^2}\right]\right\} \tag{8.18}$$

is the classic assumption for the drop size distribution in absence of additional information, because it is well known that sequential break-up processes, such as grinding of solids or disruption of droplets under mechanical agitation, lead to a log–normal distribution of particle and drop sizes, respectively [81,82]. In Equation 8.18, d_{gV} and σ are the geometric volume-based mean diameter and the width or geometric standard deviation of the distribution, respectively. The determination of the drop size distribution consists of performing a least-squares fit of the experimental data for R with Equations 8.17 and 8.18, using d_{gV} and σ as fitting parameters.

In the original work of Packer and Rees and most of the subsequent publications about this method [26,37,59–65,73,83], Equations 8.17 and 8.18 are expressed in terms of the number-based drop size distribution $p_N(a)$. It can be shown that if $p_V(a)$ is log–normal with characteristic parameters d_{gV} and σ, the corresponding number-based distribution $p_N(a)$ is also log–normal with the same geometric standard deviation σ and number-based mean size $d_{gN} = d_{gV} \cdot \exp(-3\sigma^2)$ [84]. Although both approaches are numerically equivalent, it is more proper to express these equations in terms of the volume-weighted distribution because the amplitude of transverse magnetization that is measured in a PGSE test is proportional to the volume of liquid present in the system as drops, and not to the number of droplets.

8.4.3.1 Range of Drop Sizes That can be Resolved via PGSE

The maximum drop size that can be determined via PGSE is related to the one-dimension root-mean-square displacement of spins undergoing free (Fickian) self-diffusion in isotropic, isothermal media during the diffusion time Δ:

$$d_{MAX} \approx \sqrt{2}\langle x^2 \rangle^{1/2} = \sqrt{2} \left\{ \int_{-\infty}^{\infty} (x - x_0)^2 \frac{\exp[-(x - x_0)^2/4Dt]}{\sqrt{4\pi D_{DP} t}} dx \Big|_{t=\Delta} \right\}^{1/2} = 2\sqrt{D\Delta} \quad (8.19)$$

Most of the molecules confined in a droplet with diameter much larger than d_{MAX} would not "feel" any restriction in their diffusion path due to the presence of the water/oil interface. For this reason, such a drop would not be sized accurately. This expression for d_{MAX} is also obtained by requiring the characteristic diffusion time in the drops with size d_{MAX} to be comparable to Δ ($t_{D,MAX} = a_{MAX}^2/D \approx \Delta$). The factor $\sqrt{2}$ has been included in Equation 8.19 to assure consistency between these two approaches.

Equation 8.19 suggests that d_{MAX} can be increased at will with Δ. However, the diffusion time must be adjusted keeping in mind that $\Delta < (T_{2,bulk})_{DP}$, with $(T_{2,bulk})_{DP}$ being the characteristic bulk relaxation time of the drop phase. Otherwise, the data will be affected by natural (bulk) and surface relaxation of the magnetization, and therefore by a reduction in the signal-to-noise ratio.

Low self-diffusivities render small values for d_{MAX}. In addition, low-mobility molecules usually exhibit short relaxation times [57] and therefore short values of Δ must be chosen in such cases. In general, it is not possible to determine droplet sizes via PGSE for drop phases exhibiting self-diffusion coefficients below 10^{-12} m^2/s [37].

An expression for the minimum drop size d_{MIN} that are measurable from PGSE data can be obtained from Equation 8.16:

$$d_{MIN} = \left(175\lambda \frac{D_{DP}}{\gamma^2 g^2 \delta_{MAX}}\right)^{1/4} \tag{8.20}$$

where $\lambda = 1 - R_{sp}(a = d_{MIN}/2, \delta = \delta_{MAX})$ is the smallest reduction of the attenuation ratio that can be reliably detected experimentally. Plausible values for λ are $0.05 \geq \lambda \geq 0.01$. δ_{MAX} is the maximum duration that is chosen for the magnetic field gradient pulse.

Denkova et al. [74] considered the usefulness of Equations 8.19 and 8.20 when performing an evaluation of the precision of the PGSTE method to measure drop sizes in emulsions as applied by Goudappel et al. [73], by comparing NMR and video-enhanced optical microscopy measurements for 27 *o/w* emulsions. Measurements for the minimum drop sizes were in agreement with predictions from Equation 8.20. It was also noted that drop sizes five times larger than those dictated by Equation 8.19 could be characterized while underestimating d_{gV} by $\sim$20%.

8.4.3.2 Resolving for Drop Size Distributions with Arbitrary Shape in Short Timeframes

An important shortcoming of the original PGSE method as published by Packer and Rees [58] is the assumption that the distribution of drop sizes is invariably described by a log–normal probability distribution function. Drop sizes are often, but not always, distributed in a log–normal fashion [84], and therefore Equation 8.18 does not provide a satisfactory fit of the PGSE data in all cases [64,85,86].

Ambrosone et al. [85] developed a numerical procedure based on a solution of the Fredholm integral equation to resolve the distribution function without assuming an analytical type in advance. The method was shown to be able to reconstruct the distribution function of a bimodal emulsion from a simulated PGSE experiment. Hollingsworth and Johns [86] applied regularization techniques to resolve for the shape of monomodal and bimodal emulsions from synthetic and experimental PGSE data. The ability to retrieve the correct distribution function was found to depend heavily on the regularization method chosen to assess the optimum regularization parameter.

In practice, direct methods to resolve for the shape of the distribution function directly from a PGSE or PGSTE experimental set may be adequate in some, but not in all, cases, since the procedure is usually applied on a small dataset of attenuation ratios. In such cases, multiple solutions may provide satisfactory fits of the data. Very long diffusion experiments aimed at acquiring large dataset of R may not be practical either, since changes in the drop size distribution may occur within the timeframe of the experiment.

Recent developments in this area point to performing PGSE and PGSTE measurements in combination or as part of successive pulsed sequences to enlarge the dataset while shortening the duration of the test. For systems exhibiting significant surface relaxivity, Peña and Hirasaki [47] proposed defining the distribution function from a CPMG test as explaind in Section 8.3.3, and use such distribution for the analysis of the PGSE dataset. In this combined CPMG-PGSE method, the surface relaxation is varied through successive iterations until the drop size distribution that is determined via CPMG renders a satisfactory fit for the PGSE dataset. In this way, both the drop size distribution with arbitrary shape and the surface relaxation at the water–oil interfaces are resolved. The typical duration for a CPMG-PGSE test is 5 min in a low-frequency spectrometer.

Buckley et al. [87] applied a pulsed sequence (Difftrain) that uses successive stimulated echoes from a single excitation pulse to measure self-diffusion at varying diffusion times Δ to characterize drop size distributions in emulsions. The fact that this technique collects and retains all spectral information from the emulsion with a single acquisition allows collecting a significant number of echoes in very short timeframes ($\sim$15 spin-echoes/sec at the conditions reported in Ref. 87). Although regularization methods are still needed to retrieve the drop size distribution function from Difftrain data, they can be applied over much larger datasets, thus improving the ability to resolve for arbitrary distribution function of the emulsion's drop sizes. These authors showed the drop size distribution of an emulsion of PDMS in water, which was calculated from a Difftrain dataset that was collected in just 4 sec. Results compared favorably with data gathered using the conventional PGSTE sequence.

8.4.3.3 Effect of Surface Relaxation on Restricted Diffusion Measurements

The effect of surface relaxation on the amplitude of the spin-echo in a diffusion experiment is not accounted for in the method to size emulsion droplets discussed in Section 8.4.3, since Equation 8.13 was derived assuming $\rho = 0$. It can be anticipated that this effect is small in a PGSE experiment performed in the fast diffusion regime, because in such regime the relaxation due to diffusion of the spins is much more significant than surface relaxation (see Equation 8.7).

Dunn and Sun [49] considered the effect of surface relaxation on the attenuation ratio R_{sp} by changing the boundary condition in the derivation by Neuman et al. [78] for the solution of the diffusion propagator of the spins P (see Eq. 11 in Neuman's paper) from:

$$D\nabla P\big|_{r=a} = 0 \tag{8.21}$$

to:

$$D\nabla P + \rho P\big|_{r=a} = 0 \tag{8.22}$$

to obtain:

$$R_{sp,\rho} = \exp\left\{-2\gamma^2 g^2 \sum_{m=1}^{\infty} \frac{1}{\alpha_m^2(\alpha_m^2 a^2 - 2 + \rho^2 a^2/D^2 - \rho a/D)}\left[\frac{2\delta}{\alpha_m^2 D} - \frac{\Psi}{(\alpha_m^2 D)^2}\right]\right\} \tag{8.23}$$

where Ψ is given by Equation 8.14 as before and α_m is the m^{th} positive root of the equation:

$$\alpha a \cdot J_{5/2}(\alpha a) - \left(1 + \frac{\rho a}{D}\right) J_{3/2}(\alpha a) = 0 \tag{8.24}$$

Equation 8.23 applies only for small ρ and large D so the probability of finding a spin anywhere in the drop is nearly uniform and the GPD approximation is satisfied (see discussion following Equation 8.16). Otherwise, significant surface relaxation would take place and a non-Gaussian distribution of the phase shifts of the spins near the water/oil interfaces would be observed. Equation 8.23 reduces to Equation 8.13 in the limit $\rho a/D \to 0$, as might be expected.

Codd and Callaghan [88] extended a matrix formalism developed by Callaghan [89] to interpret restricted diffusion data from pulsed sequences with gradient pulses of arbitrary shape, to take into account surface relaxation at the walls of spheres. These authors noted that when $\rho = 1$

to 10 μm/s and the magnetization data is collected from pores of the order of 10 μm, the effect of surface relaxation on the attenuation ratio can be neglected. This assessment can be confirmed in a straightforward manner via Equation 8.23.

8.4.4 A Generalized Theory for the Time-Resolved Attenuation Ratio of Emulsions

Packer and Rees [58] pointed out that the procedure described in Section 8.4.3 is useful to determine the drop size distribution whenever the spin-echo is originated solely from the drop phase of the emulsion. This is

$$R_{EMUL} = R_{DP} \tag{8.25}$$

where R_{EMUL} and R_{DP} are the attenuation ratio that is measured for the emulsion and for the drop phase, respectively. This assumption limits the applicability of the method to emulsions for which the signal from the continuous phase is suppressed (i.e., emulsions of oil in D_2O). Equation 8.25 is also valid if the transverse magnetization of the continuous phase has relaxed completely and the natural (bulk) relaxation of the drop phase is small at the time the spin-echo is acquired. Namely,

$$(T_{2,bulk})_{CP} \ll 2\tau \ll (T_{2,bulk})_{DP} \tag{8.26}$$

where $(T_{2,bulk})_{CP}$ is the characteristic bulk relaxation time of the continuous phase. Equation 8.26 is often satisfied by emulsions of water in viscous oils, but not by emulsions of viscous oils in water. This explains why the PGSE method was often applied during the last 30 years for the determination of drop sizes in *w/o* emulsions such as margarine, butter, and low-calorie spreads [59,60,62,83,90] and water-in-crude-oil emulsions [61], but not as often for the characterization of *o/w* emulsions [73,74].

The impossibility of resolving for the drop size distributions, when the contribution of the magnetization of the continuous phase to the spin-echo is significant, was overcome with the introduction of the Fourier-transform PGSE method (FT-PGSE). Excellent reviews on this method and its applications in the characterization of water/oil/surfactant systems have been published by Stilbs [24] and Söderman and Stilbs [25]. In the FT-PGSE procedure, the second half of the spin-echo that is generated in the PGSE sequence is Fourier-transformed, and the individual contributions of the components to the spin-echo appear as separate peaks in the frequency domain due to differences in self-diffusivity. Lönnqvist et al. [26] applied this technique to resolve for the individual signal of water and oil in simple (*w/o*) and multiple (*w/o/w*) emulsions. Ambrosone et al. [90] used the method to isolate the water signal from margarine and emulsions of water in olive oil.

Better resolution of the Fourier spectrum is attained as the strength of the magnetic field is increased. For this reason, high-resolution magnets with frequencies typically above 80 MHz are used in FT-PGSE studies. Unfortunately, individual peaks cannot be resolved satisfactorily at the frequencies at which low-resolution NMR spectrometers operate (~ 2 to 20 MHz). Therefore, the determination of the individual contributions of water and oil to the spin-echo that is obtained from an emulsion in the time domain is relevant, particularly for industrial applications in which high-resolution spectrometers cannot be afforded.

A generalized expression for the time-resolved attenuation ratio of emulsions was reported recently [47]:

$$R_{EMUL} = (1-\kappa)R_{DP} + \kappa R_{CP}; \quad 0 \le \kappa \le 1 \tag{8.27}$$

where R_{CP} is the time-resolved attenuation ratios of the continuous phase, respectively. κ is a parameter associated with the natural relaxation of the transverse component of the magnetization of both phases as shown later. R_{DP} is given by Equation 8.17 as before, and $R_{sp}(a)$ is calculated using Equation 8.13. Diffusion in the continuous phase may occur as bulk diffusion ($R_{CP} \sim R_{bulk,CP}$), particularly for dilute emulsions. In such a case, R_{CP} can be calculated using Equation 8.12. The case in which restricted diffusion in the continuous phase due to the presence of droplets significantly affects R_{CP} has also been considered [47,91].

In general, κ is given by:

$$\kappa = \left[1 + \frac{M_{xy,DP}(t_{SE}, g=0)}{M_{xy,CP}(t_{SE}, g=0)}\right]^{-1} \tag{8.28}$$

where t_{SE} is the time for maximal amplitude of the spin-echo, and $M_{xy,DP}(t_{SE}, g=0)$ and $M_{xy,CP}(t_{SE}, g=0)$ are the magnitudes of the transverse component of the magnetization vector at time t_{SE} when $g=0$ for the drop and continuous phase, respectively. For the basic PGSE sequence (Figure 8.6(a)), $t_{SE} = 2\tau$ and Equation 8.28 becomes:

$$\kappa = \left[1 + \frac{\sum(f_i)_{DP}\exp[-2\tau/(T_{2,i})_{DP}]}{\sum(f_i)_{CP}\exp[-2\tau/(T_{2,i})_{CP}]}\right]^{-1} \simeq \left[1 + \frac{\phi_{DP}}{\phi_{CP}}\frac{HI_{DP}}{HI_{CP}}\frac{\exp[-2\tau/(T_{2,bulk})_{DP}]}{\exp[-2\tau/(T_{2,bulk})_{CP}]}\right]^{-1} \tag{8.29}$$

where the $T_{2,i} - f_i$ values for each phase are determined from the T_2 distribution of the emulsion via CPMG as explained above. For the PGSTE sequence (Figure 8.6(b)), $t_{SE} = 2\tau + T$ and κ becomes:

$$\begin{aligned}\kappa &= \left[1 + \frac{\sum(f_i)_{DP}\exp[-2\tau/(T_{2,i})_{DP} - T/(T_{1,i})_{DP}]}{\sum(f_i)_{CP}\exp[-2\tau/(T_{2,i})_{CP} - T/(T_{1,i})_{CP}]}\right]^{-1} \\ &\cong \left[1 + \frac{\phi_{DP}}{\phi_{CP}}\frac{HI_{DP}}{HI_{CP}}\frac{\exp[-2\tau/(T_{2,bulk})_{DP} - T/(T_{1,bulk})_{DP}]}{\exp[-2\tau/(T_{2,bulk})_{CP} - T/(T_{1,bulk})_{CP}]}\right]^{-1}\end{aligned} \tag{8.30}$$

assuming that the ratio $T_{1,i}/T_{2,i} = T_{1,bulk}/T_{2,bulk}$ remains constant. Surface relaxation effects are neglected for the approximations made in Equations 8.29 and 8.30.

According to Equation 8.28, $\kappa \to 0$ when the signal of the continuous phase is suppressed, or when it has relaxed completely at the time the spin-echo is acquired. If so, Equation 8.27 reduces to Equation 8.25. It is inferred from this analysis that the classic method to interpret NMR PGSE data in the time domain to calculate drop sizes is valid only whenever $\kappa \to 0$. Neglecting the effect of κ may lead to significant errors in the interpretation of PGSE data in the time domain as shown below.

Figure 8.8 shows (circles) experimental data for a sample containing water (10 vol%) and a crude oil (90 vol%) in contact as bulk fluids, and for a *w/o* emulsion (squares) made from the same water/crude oil mixture [47]. The emulsion was ultrasonicated until the drop sizes were

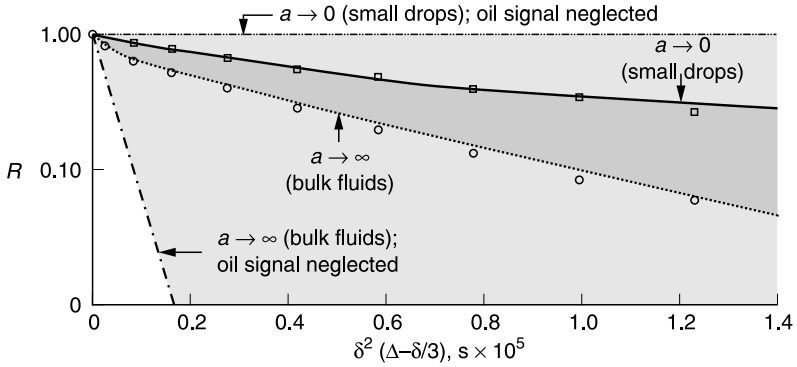

FIGURE 8.8 Effect of the transverse magnetization of the continuous phase on the PGSE response of mixtures of water and crude oil, contacted as bulk fluids and emulsified.

below the resolution limit of the PGSE experiment, which was $d_{MIN} \sim 3$ μm, according to Equation 8.20. The mean drop size was followed via microphotography, and the final emulsion exhibited a narrow distribution of droplets with sizes close to 0.5 μm. Since water is dispersed as droplets, Equation 8.27 becomes $R_{EMUL} = (1 - \kappa)R_W + \kappa R_O$. In this case, $\kappa = 0.755$ was calculated from Equation 8.29, which indicates that 75.5% of the attenuation ratio of the mixture was determined by the oil phase.

The dotted curve in Figure 8.8 shows the predicted behavior for the sample before emulsification using Equation 8.27 with $R_{DP} = R_{bulk,DP}$ and $R_{CP} = R_{bulk,CP}$. The predicted behavior for the attenuation ratio of the emulsion via Equation 8.27 is also shown (continuous line). R_O was calculated using Equation 8.12 and considering the distribution of diffusion coefficients in the oil phase as described in Ref. 47, whereas $R_W \sim 1$ according to Equation 8.16. The excellent agreement between experiments and calculations shows that Equation 8.27 is valid both for mixtures of bulk fluids and emulsions.

The dash–dot and dash–dot–dot lines in Figure 8.8 stand for the attenuation profiles that would be obtained for the same system before and after emulsification, respectively, if the contribution of the oil signal to the spin-echo amplitude is neglected. The area of the plot between these two lines has been shaded in light tone to indicate the range of conditions in which the attenuation ratios for emulsions with any given drop size distribution could be found if the oil signal were indeed negligible, i.e., if Equation 8.25 were correct. If Equation 8.27 holds instead as experiments suggest, such conditions are restricted to the area shaded in dark tone. Clearly, neglecting the signal from the oil phase could lead to significant error in the prediction of the attenuation profile for this system. The trends shown in Figure 8.8 have been confirmed in experiments with other water/oil mixtures [47].

It is worth noting that the parameters of a PGSE or PGSTE experiment should be chosen in order to *minimize* the effect of the continuous phase on the spin-echo and therefore on the attenuation ratio of the emulsion, while maintaining a satisfactory signal-to-noise ratio. The idea is to broaden the range of conditions at which attenuation ratios can be obtained (that is, to expand the extension of the dark-shaded area in Figure 8.8), so the uncertainty in the drop size distribution that is determined from the PGSE diminishes. Therefore, Equation 8.27 can be used as a tool to predict limiting attenuation profiles and optimize the selection of parameters for testing.

8.4.5 Other Applications of NMR Diffusion Measurements

Diffusion experiments have been used not only to size droplets in emulsions, but also pores in mineral samples [67,92,93], biological cells and heterogeneities in organic tissue [94,95]. The three-dimensional packing of compressed drops in highly concentrated emulsions ($\phi_{DP} \sim 1$) has also been studied with this method [75,96]. Micelles, bicontinuous structures in microemulsions, vesicles and liquid crystals in surfactant/oil/water/systems have also been characterized with these techniques [62,97–100]. Novel NMR applications in relation to emulsions continue to appear in the general literature, of which a few illustrative examples are briefly described below.

8.4.5.1 Characterization of Emulsions in Flow

The conventional PGSE and PGSTE pulsed sequences cannot be used in emulsions in flow because both self-diffusion and velocity contribute to the attenuation of magnetization in the presence of field gradients. A flow-compensating PGSTE pulsed sequence was introduced by Johns and Gladden [65] and used to characterize xylene-in-water emulsions in laminar flow. In essence, this sequence halves the diffusion time Δ by adding two rf 90° pulses sandwiched between two additional gradient pulses to the classic PGSTE sequence. The flow effect is compensated whenever the assumption that the displacement of each individual molecule during the initial diffusion time $\Delta/2$ is equivalent to the displacement of such molecule due to the second $\Delta/2$ time period is valid. Therefore, only emulsions in laminar flow exhibiting negligible diffusion in the direction transverse to the flow are suited for evaluation. Figure 8.9(a) shows a comparison of the drop size distributions that were measured in a quiescent emulsion using confocal microscopy, the conventional PGSTE sequence, and the flow-compensating PGSTE sequence. Excellent agreement was found among results from the three techniques, thus showing that the modification to the pulsed sequence does not affect the ability to quantify for drop sizes. Figure 8.9(b) shows results for the drop size distribution of the emulsion under flow at two different superficial velocities. It is seen that an increase in velocity resulted in narrower drop size distributions with smaller mean sizes. The effect was attributed to breakage of larger drops into smaller drops as the superficial velocity was increased.

8.4.5.2 Kinetics of Emulsion Freezing

NMR has also been used to characterize emulsions undergoing freezing and freeze/thaw cycling. For such application, NMR proves to be particularly useful since it allows identifying changes in the physical state not only of the water and oil phases, but also of components within each of such phases during cooling/heating processes.

Hindmarsh et al. [71] followed the freezing behavior of drops containing emulsions of hydrocarbons in water and water/sucrose mixtures using the PGSTE technique. Figure 8.10(a) shows the transient behavior of the intensity of the NMR signal for the water, sucrose, and dodecane that were present in an emulsion sample of 20 wt% dodecane-in-20 wt% sucrose solution at −40°C. The plots indicate that nucleation of water, sucrose, and dodecane started at about 35, 65, and 80 sec after subjecting the emulsion sample to cooling, respectively. Interestingly, the NMR data captures the fact that an inflexion in the water curve appeared once the nucleation of sucrose started, while an inflexion in the sucrose curve appears when the nucleation for dodecane began. These phenomena are due to a reduction in the freezing rate whenever latent heat is released by a component for which nucleation begins. Figure 8.10(b) shows the drop size distribution of the same emulsion described above, first unfrozen and then cooled down to temperatures at which freezing of the drop phase (dodecane) would not occur. The inserted plot reports the same data

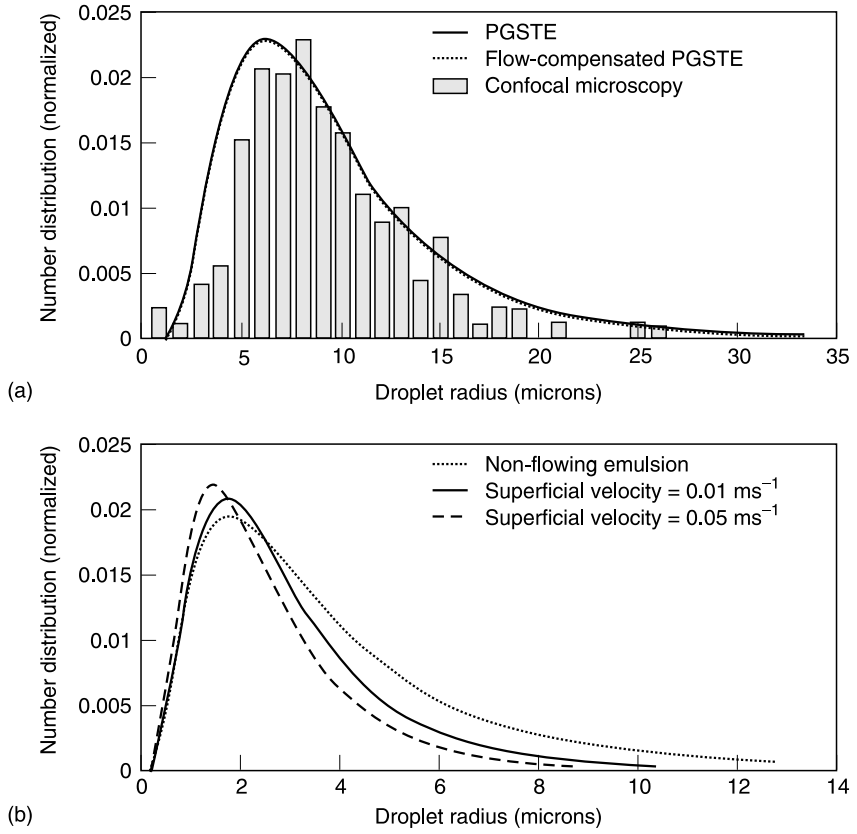

FIGURE 8.9 (a) Comparison of drop size distribution measurements from PGSTE, flow-compensated PGSTE, and optical microscopy for a quiescent water-in-oil emulsion; (b) flow-compensated PGSTE measurements for the distribution of drop sizes of emulsions in flow. (Adapted from Ref. 65.)

for a dodecane-in-water emulsion for which sucrose was not added. These data suggest that the presence of sucrose inhibits the coalescence and growth of droplet sizes when freezing the emulsion. This assessment confirms previous studies reporting a stabilizing effect of water-soluble carbohydrates in *o/w* emulsions subject to freezing [101,102].

8.4.6 Advantages and Limitations of the PGSE and PGSTE Experiments

In the PGSE and PGSTE methods, the contributions of the water and oil phases to the attenuation ratio R can be resolved independently. Also, surface relaxation has a negligible effect on R in the fast diffusion regime and therefore the PGSE and PGSTE data can be interpreted solely in terms of self-diffusivity and natural (bulk) relaxation. As a result, an independent measurement of the drop size distribution, and therefore of the surface-to-volume ratio of the drop phase in the emulsion, can be obtained with these procedures.

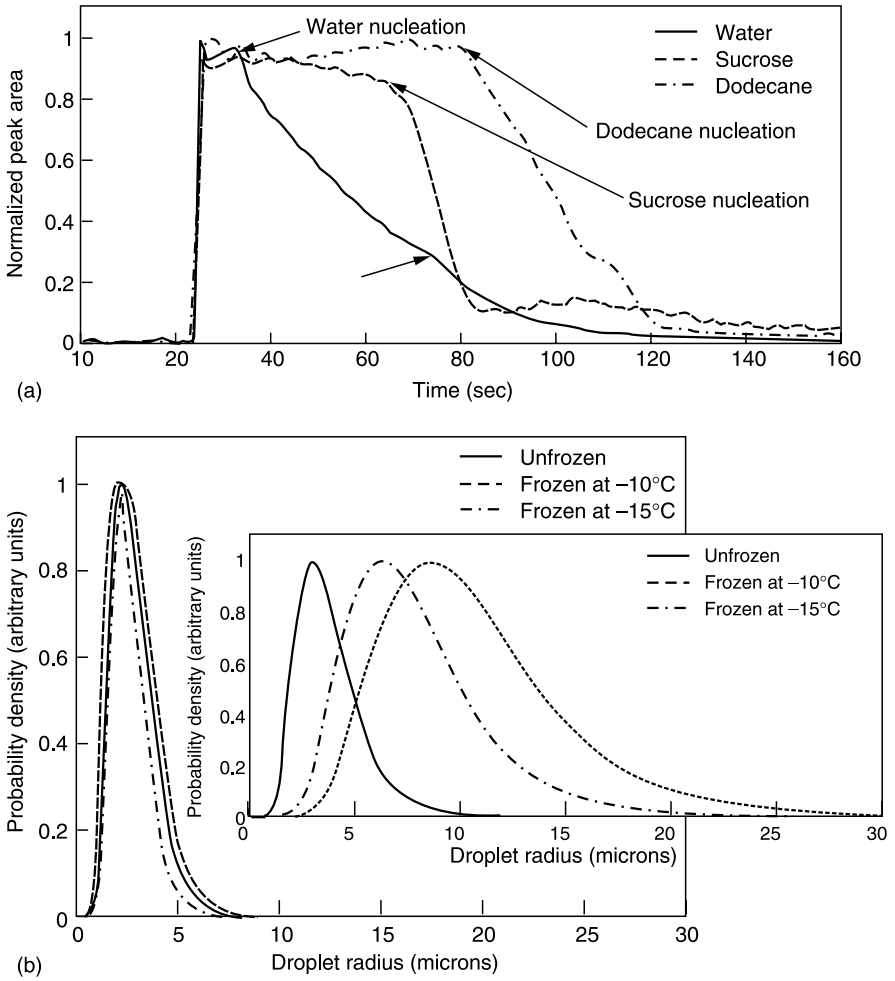

FIGURE 8.10 (a) NMR signal of the components present in an emulsion undergoing freezing; (b) NMR-resolved drop size distributions of freezing emulsions. (Adapted from Ref. 71.)

Nevertheless, the range of drop sizes that can be determined precisely with these methods is narrow (~1 to 50 μm). Furthermore, the PGSE and PGSTE experiments are slow: acquiring a dataset comparable to that of a single CPMG test would take several days. For this reason, in a typical PGSE experiment only few (~10 to 20) attenuation ratios are measured in 5 to 20 min. Due to lack of data, the drop size distribution is resolved assuming in advance a p.d.f. to describe it. Recent studies have unveiled the possibility of combining diffusion and relaxation experiments to overcome these limitations [47,87].

REFERENCES

1. Friberg, S.E., K. Larsson, and J. Sjöblom, Eds. *Food Emulsions*. 4th Edition. 2003, Marcel Dekker, Inc.: New York.
2. McClements, D.J., *Food Emulsions: Principles, Practices and Techniques*. 2nd Edition. 2004, CRC Press: Boca Raton, USA.

3. Rieger, M.M. and L.D. Rhein, Eds. *Surfactants in Cosmetics*. 2nd Edition. 1997, Marcel Dekker, Inc.: New York.
4. Nielloud, F. and G. Marti-Mestres, Eds. *Pharmaceutical Emulsions and Suspensions*. 2000, Marcel Dekker, Inc.: New York.
5. Turner, G.P.A. and J. Bentley, *Introduction to Paint Chemistry and Principles of Paint Technology*. 4th Edition. 1997, CRC Press: Boca Raton, USA.
6. Foy, C.L. and D.W. Pritchard, Eds. *Pesticide Formulation and Adjuvant Technology*. 1996, CRC Press: Boca Raton, USA.
7. Becher, P., *Emulsions: Theory and Practice*. 3rd Edition. 2001, Oxford University Press: New York.
8. Muncy, H.W., *Asphalt Emulsions*. ASTM Special Technical Publications # 1079. 1990, ASTM International: West Conshohoker, USA.
9. Schramm, L.L., *Emulsions: Fundamentals and Applications in the Petroleum Industry*. Advances in Chemistry. Vol. #231. 1992, American Chemical Society: Washington D.C.
10. Sjöblom, J., N. Aske, I.H. Auflem, O. Brandal, T. Havre, O. Saether, A. Westvik, E.E. Johnsen, and H. Kallevik, Our Current Understanding of Water-in-Crude Oil Emulsions. Recent Characterization Techniques and High Pressure Performance. *Advances in Colloid and Interface Science*, (2003). **100–102**: pp. 399–473.
11. Hartland, S. and S. Jeelani, Gravity settlers, in *Liquid–liquid Extraction Equipment*, J.C. Godfrey and M.J. Slater, Editors. 1994, John Wiley & Sons: New York.
12. Otsubo, Y. and R.K. Prud'homme, Effect of drop size distribution on the flow behavior of oil-in-water emulsions. *Rheologica Acta*, (1994). **33**(4): pp. 303–306.
13. Ramírez, M., J. Bullón, J. Andérez, I. Mira, and J.L. Salager, Drop size distribution and its effect on O/W emulsion viscosity. *Journal of Dispersion Science and Technology*, (2002). **23**(1–3): pp. 309–321.
14. Pal, R., Effect of droplet size on the rheology of emulsions. *AIChE Journal*, (1996). **42**(11): pp. 3181–3190.
15. Walstra, P., *Emulsion stability*, in *Encyclopedia of Emulsion Technology*, Volume 4, P. Becher, Editor. 1996, Marcel Dekker, Inc.: New York. Chapter 1.
16. Peña, A.A. and C.A. Miller, Transient behavior of polydisperse emulsions undergoing mass transfer. *Industrial and Engineering Chemistry Research*, (2002). **41**(25): pp. 6284–6296.
17. McClements, D.J., Theoretical prediction of emulsion color. *Advances in Colloid and Interface Science*, (2002). **97**: pp. 63–89.
18. Kilcast, D. and S. Clegg, Sensory perception of creaminess and its relationship with food structure. *Food Quality and Preferences*, (2002). **13**: pp. 609–623.
19. Lissant, K., *Demulsification: Industrial Applications*. 1983, Marcel Dekker, Inc.: New York.
20. Orr, C., *Determination of Particle Size*, in *Encyclopedia of Emulsion Technology*, Vol. 3, Chapter 3, P. Becher, Editor. 1988, Marcel Dekker, Inc.: New York.
21. Sjöblom, J., Ed. *Encyclopedic Handbook of Emulsion Technology*. 2001, Marcel Dekker, Inc.: New York. pp. 736.
22. Coupland, J.N. and D.J. McClements, *Analysis of Droplet Characteristics Using Low-Intensity Ultrasound*, in *Food Emulsions*, S.E. Friberg, K. Larsson, and J. Sjöblom, Editors. 2003, Marcel Dekker, Inc.: New York.
23. Callaghan, P., *Principles of Nuclear Magnetic Resonance Microscopy*. 1991, Oxford University Press: New York. pp. 492.
24. Stilbs, P., Fourier transform pulsed-gradient spin-echo studies of molecular diffusion. *Progress in NMR Spectroscopy*, (1987). **19**: pp. 1–45.
25. Söderman, O. and P. Stilbs, NMR studies of complex surfactant systems. *Progress in NMR Spectroscopy*, (1994). **26**: pp. 445–482.
26. Lönnqvist, I., B. Hakansson, B. Balinov, and O. Söderman, NMR self-diffusion studies of the water and the oil components in a W/O/W emulsion. *Journal of Colloid and Interface Science*, (1997). **192**(1): pp. 66–73.
27. Parhami, P. and B.M. Fung, Fluorine-19 relaxation study of perfluorochemicals as oxygen carriers. *Journal of Physical Chemistry*, (1983). **87**: pp. 1928–1931.

28. Schnur, G., R. Kimmich, and R. Lietzenmayer, Hydrogen/fluorine retuning tomography. Applications to ^{1}H image-guided volume-selective ^{19}F spectroscopy and relaxometry of perfluorocarbon emulsions in tissue. *Magnetic Resonance in Medicine*, (1990). **13**(3): pp. 478–489.
29. Chiba, K. and M. Tada, Study of the emulsion stability and headgroup motion of phosphatidylcholine and lysophosphatidylcholine by carbon-13 and phosphorus-31. *Agric. Biol. Chem.*, (1989). **53**: pp. 995–1001.
30. Rotenberg, M., M. Rubin, A. Bor, D. Meyuhas, Y. Talmon, and D. Lichtenberg, Physico-chemical characterization of intralipid emulsions. *Biochim. Biophys. Acta*, (1991). **1086**(3): pp. 265–272.
31. Drew, J., A. Liodakis, R. Chan, H. Du, M. Sadek, R. Brownlee, and W.H. Sawyer, Preparation of lipid emulsions by pressure extrusion. *Biochem. Int.*, (1990). **22**(6): pp. 983–992.
32. Férézou, J., T.L. Nguyen, C. Leray, T. Hajri, A. Frey, Y. Cabaret, J. Courtieu, C. Lutton, and A.C. Bach, Lipid composition and structure of commercial parenteral emulsions. *Biochim. Biophys. Acta*, (1994). **1213**(2): pp. 149–158.
33. Westesen, K. and T. Wehler, Investigation of the particle size of a model intravenous emulsion. *J. Pharm. Sci.*, (1993). **82**(12): pp. 1237–1244.
34. ter Beek, L.C., K. Ketelaars, D.C. McGain, P.E. Smulders, P. Walstra, and M.A. Hemminga, Nuclear magnetic resonance study of the conformation and dynamics of beta-casein at the oil/water interface in emulsions. *Biophys. J.*, (1996). **70**(5): pp. 2396–2402.
35. Wolber, J., I. Rowland, M. Leach, and A. Bifone, perfluorocarbon emulsions as intravenous delivery media for hyperpolarized xenon. *Magnetic Resonance in Medicine*, (1999). **41**(3): pp. 442–449.
36. Möller, H.E., M.S. Chawla, X.J. Chen, B. Driehuys, L.W. Hedlund, C.T. Wheeler, and G.A. Johnson, Magnetic resonance angiography with hyperpolarized 129-Xe dissolved in a lipid emulsion. *Magnetic Resonance in Medicine*, (1999). **41**(5): pp. 1058–1064.
37. Balinov, B. and O. Söderman, *Emulsions – the NMR perspective*, in *Encyclopedic Handbook of Emulsion Technology*, J. Sjöblom, Editor. 2001, Marcel Dekker, Inc.: New York.
38. Håkansson, B., O. Söderman, and B. Balinov, *Nuclear Magnetic Resonance of Emulsions*, in *Encyclopedia of Surface and Colloid Science*, A.T. Hubbard, Editor. 2002, Marcel Dekker, Inc.: New York. pp. 3684–3699.
39. Carr, H.Y. and E.M. Purcell, Effects of diffusion on free precession in nuclear magnetic resonance experiments. *Physical Review*, (1954). **94**(3): pp. 630–638.
40. Meiboom, S. and D. Gill, Modified spin-echo method for measuring nuclear relaxation times. *The Review of Scientific Instruments*, (1959). **29**(8): pp. 688–691.
41. Tikhonov, A.N. and V.Y. Arsenin, *Solution of Ill-posed Problems*. 1977, Winston & Sons: Washington D.C. pp. 258.
42. Dunn, K.J., G.A. LaTorraca, J.L. Warner, and D.J. Bergman. *On the Calculation and Interpretation of NMR Relaxation Times Distribution, SPE Paper 28367*. In: 69th Annual SPE Technical Conference and Exhibition. 25–28 September 1994. New Orleans, USA.
43. LaTorraca, G.A., K.J. Dunn, P.R. Webber, and R.M. Carlson, Low-field NMR determinations of the properties of heavy oils and water-in-oil emulsions. *Magnetic Resonance Imaging*, (1998). **16**(5–6): pp. 659–662.
44. Cannon, D.E., C. Cao Minh, and R.L. Kleinberg. *Quantitative NMR interpretation*. In: SPE Annual Technical Conference and Exhibition. SPE Paper 49010, September 27–30, 1998. New Orleans, USA.
45. Zhang, Q., S.W. Lo, C.C. Huang, and G.J. Hirasaki. *Some exceptions to the default NMR rock and fluid properties*. In: SPWLA 39th Annual Logging Symposium. May 25–28, 1998. Keystone, Colorado.
46. Kleinberg, R.L. and H.J. Vinegar, NMR properties of reservoir fluids. *The Log Analyst*, (1996). **37**(6): pp. 20–32.
47. Peña, A.A. and G.J. Hirasaki, Enhanced characterization of oilfield emulsions via NMR diffusion and transverse relaxation experiments. *Advances in Colloid and Interface Science*, (2003). **105**: pp. 103–150.
48. Allsopp, K., I. Wright, D. Lastockin, K. Mirotchnik, and A. Kantzas, Determination of oil and water compositions of oil/water emulsions using low field NMR relaxometry. *Journal of Canadian Petroleum Technology*, (2001). **40**(7): pp. 58–61.

49. Dunn, K.J. and B. Sun, Personal communication. 2002.
50. Hills, B.P., H.R. Tang, P. Manoj, and C. Destruel, NMR diffusometry of oil-in-water emulsions. *Magnetic Resonance Imaging*, (2001). **19**(3–4): pp. 449–451.
51. Clark, B. and R.L. Kleinberg, Physics in oil exploration. *Physics Today*, (2002). **April**: pp. 48–53.
52. Kenyon, W.E., Nuclear magnetic resonance as a petrophysical measurement. *Nuclear Geophysics*, (1992). **6**(2): pp. 153–171.
53. Matteson, A., J.P. Tomanic, M.M. Herron, D.F. Allen, and W.E. Kenyon, NMR relaxation of clay/brine mixtures. *SPE Reservoir Evaluation & Engineering*, (2000). **3**(5): pp. 408–413.
54. Logan, W.D., J.P. Horkowitz, R. Laronga, and D.W. Cromwell, Practical application of NMR logging in carbonate reservoirs. *SPE Reservoir Evaluation & Engineering*, (1998). **1**(5): pp. 438–448.
55. Brownstein, K.R. and C.E. Tarr, Importance of classical diffusion in NMR studies of water in biological cells. *Physical Review A*, (1979). **19**(6): pp. 2446–2453.
56. Flaum, M., J. Chen, and G.J. Hirasaki, NMR diffusion editing for D-T_2 maps: Application to recognition of wettability change. *Petrophysics*, (In press).
57. Freedman, R., S.W. Lo, M. Flaum, G.J. Hirasaki, A. Matteson, and A. Sezginer, A new NMR method of fluid characterization in reservoir rocks: experimental confirmation and simulation results. *SPE Journal*, (2001). **December**: pp. 452–464.
58. Packer, K.J. and C. Rees, Pulsed NMR studies of restricted diffusion. I. droplet size distribution in emulsions. *Journal of Colloid and Interface Science*, (1972). **40**(2): pp. 206–218.
59. Van Den Enden, J.C., D. Waddington, H. Vanaalst, C.G. Vankralingen, and K.J. Packer, Rapid determination of water droplet size distributions by PFG-NMR. *Journal of Colloid and Interface Science*, (1990). **140**(1): pp. 105–113.
60. Balinov, B., O. Söderman, and T. Warnheim, Determination of water droplet size in margarines and low-calorie spreads by nuclear-magnetic-resonance self-diffusion. *Journal of the American Oil Chemists Society*, (1994). **71**(5): pp. 513–518.
61. Balinov, B., O. Urdahl, O. Söderman, and J. Sjöblom, Characterization of water-in-crude-oil emulsions by the NMR self-diffusion technique. *Colloids and Surfaces A – Physicochemical and Engineering Aspects*, (1994). **82**(2): pp. 173–181.
62. Söderman, O., I. Lönnqvist, and B. Balinov, *NMR Self-diffusion Studies of Emulsion Systems. Droplet Sizes and Microstructure of the Continuous Phase*, in *Emulsions – a Fundamental and Practical Approach*, J. Sjöblom, Editor. 1992, Kluwer Academic Publishers: The Netherlands. pp. 239–258.
63. Fourel, I., J.P. Guillement, and D. Le Botlan, Determination of water droplet size distributions by low-resolution PFG-NMR 1. "Liquid" emulsions. *Journal of Colloid and Interface Science*, (1994). **164**(1): pp. 48–53.
64. Lee, H.Y., M.J. McCarthy, and S.R. Dungan, Experimental characterization of emulsion formation and coalescence by nuclear magnetic resonance restricted diffusion techniques. *Journal of the American Oil Chemists' Society*, (1998). **75**(4): pp. 463–475.
65. Johns, M.L. and L.F. Gladden, Sizing of emulsion droplets under flow using flow-compensating NMR-PFG techniques. *Journal of Magnetic Resonance*, (2002). **154**(1): pp. 142–145.
66. Peña, A.A., G.J. Hirasaki, and C.A. Miller, Chemically induced destabilization of water-in-crude oil emulsions. *Industrial and Engineering Chemistry Research*, (2005), **44**(15): pp. 1139–1149.
67. Tanner, J.E. and E.O. Stejskal, Restricted self-diffusion of protons in colloidal systems by the pulsed-gradient, spin-echo method. *The Journal of Chemical Physics*, (1968). **49**(4): pp. 1768–1777.
68. Stejskal, E.O. and J.E. Tanner, Spin diffusion measurements: spin echoes in the presence of a time-dependent field gradient. *The Journal of Chemical Physics*, (1965). **42**(1): pp. 288–292.
69. Tanner, J.E., Use of the stimulated echo in NMR diffusion studies. *The Journal of Chemical Physics*, (1970). **52**(5): pp. 2523–2526.
70. Hedin, N. and I. Furó, Ostwald Ripening of an Emulsion Monitored by PGSE NMR. *Langmuir*, (2001). **17**(16): pp. 4746–4752.
71. Hindmarsh, J.P., K.G. Hollingsworth, D.I. Wilson, and M.L. Johns, An NMR study of the freezing of emulsion-containing drops. *Journal of Colloid and Interface Science*, (2004). **275**: pp. 165–171.
72. Garasanin, T. and T. Cosgrove, NMR Self-Diffusion Studies on PDMS oil-in-water emulsion. *Langmuir*, (2002). **18**: pp. 10298–10304.

73. Goudappel, G.J.W., J.P.M. van Duynhoven, and M.M.W. Mooren, Measurement of oil droplet size distributions in food oil/water emulsions by time domain pulsed field gradient NMR. *Journal of Colloid and Interface Science*, (2001). **239**: pp. 535–542.
74. Denkova, P.S., S. Tcholakova, N.D. Denkov, K.D. Danov, B. Campbell, C. Shawl, and D. Kim, Evaluation of the precision of drop-size determination in oil/water emulsions by low-resolution NMR spectroscopy. *Langmuir*, (2004). **20**: pp. 11402–11413.
75. Håkansson, B., R. Pons, and O. Söderman, Structure determination of a highly concentrated W/O emulsion using pulsed-field-gradient spin-echo nuclear magnetic resonance "diffusion diffractograms." *Langmuir*, (1999). **15**(4): pp. 988–991.
76. Mezzenga, R., B.M. Folmer, and E. Hughes, Design of double emulsions by osmotic pressure tailoring. *Langmuir*, (2004). **20**: pp. 3574–3582.
77. Robertson, B., Spin-echo decay of spins diffusing in a bounded region. *Physical Review*, (1966). **151**(1): pp. 273–277.
78. Neuman, C.H., Spin echo of spins diffusing in a bounded medium. *The Journal of Chemical Physics*, (1974). **60**(11): pp. 4508–4511.
79. Murday, J.S. and R.M. Cotts, Self-diffusion coefficient of liquid lithium. *The Journal of Chemical Physics*, (1968). **48**(11): pp. 4938–4945.
80. Balinov, B., B. Jönsson, P. Linse, and O. Söderman, The NMR self-diffusion method applied to restricted diffusion – simulation of echo attenuation from molecules in spheres and between planes. *Journal of Magnetic Resonance Series A*, (1993). **104**(1): pp. 17–25.
81. Epstein, B., Logarithmico-normal distribution in breakage of solids. *Industrial and Engineering Chemistry*, (1948). **40**(12): pp. 2289–2290.
82. Salager, J.L., M. Pérez-Sénchez, M. Ramírez-Gouveia, J.M. Andérez, and M.I. Briceño-Rivas, Stirring-formulation coupling in emulsions. *Récent Progrès en Génie des Procédés*, (1997). **11**(52): pp. 123–130.
83. Fourel, I., J.P. Guillement, and D. Le Botlan, Determination of water droplet size distributions by low-resolution PFG-NMR. 2. Solid emulsions. *Journal of Colloid and Interface Science*, (1995). **169**(1): pp. 119–124.
84. Orr, C., *Emulsion Droplet Size Data*, in *Encyclopedia of Emulsion Technology*, 1, P. Becher, Editor. 1983, Marcel Dekker, Inc.: New York. pp. 369–404.
85. Ambrosone, L., G. Colafemmina, M. Giustini, G. Palazzo, and A. Ceglie, Size distribution in emulsions. *Progress in Colloid and Polymer Science*, (1999). **112**: pp. 86–88.
86. Hollingsworth, K.G. and M.L. Johns, Measurement of emulsion droplet sizes using PFG NMR and regularization methods. *Journal of Colloid and Interface Science*, (2003). **258**: pp. 383–389.
87. Buckley, C., K.G. Hollingsworth, A.J. Sederman, D.J. Holland, M.L. Johns, and L.F. Gladden, Applications of fast diffusion measurement using Difftrain. *Journal of Magnetic Resonance*, (2003). **161**: pp. 112–117.
88. Codd, S.L. and P.T. Callaghan, Spin echo analysis of restricted diffusion under generalized gradient waveforms: Planar, cylindrical and spherical pores with wall relaxivity. *Journal of Magnetic Resonance*, (1999). **137**: pp. 358–372.
89. Callaghan, P., A simple matrix formalism for spin echo analysis of restricted diffusion under generalized gradient waveforms. *Journal of Magnetic Resonance*, (1997). **129**: pp. 74–84.
90. Ambrosone, L., A. Ceglie, G. Colafemmina, and G. Palazzo, NMR studies of food emulsions: the dispersed phase self-diffusion coefficient calculated by the least variance method. *Progress in Colloid and Polymer Science*, (2000). **115**: pp. 161–165.
91. Liu, E.-H., P. Callaghan, and K.M. McGrath, Bicontinous and closed-cell foam emulsions as continuum structures in an oil in water emulsion system. *Langmuir*, (2003). **19**: pp. 7249–7258.
92. Bergman, D.J. and K.J. Dunn, Theory of diffusion in a porous-medium with applications to pulsed-field-gradient NMR. *Physical Review B*, (1994). **50**(13): pp. 9153–9156.
93. Hürlimann, M.D., K.G. Helmer, L.L. Latour, and C.H. Sotak, Restricted diffusion in sedimentary-rocks – Determination of surface-area-to-volume ratio and surface relaxivity. *Journal of Magnetic Resonance Series A*, (1994). **111**(2): pp. 169–178.
94. Topgaard, D. and O. Söderman, Diffusion of water absorbed in cellulose fibers studied with ^{1}H-NMR. *Langmuir*, (2001). **17**(9): pp. 2694–2702.

95. Ngwa, W., O. Geier, L. Naji, J. Schiller, and K. Arnold, Cation diffusion in cartilage measured by pulsed field gradient NMR. *European Biophysics Journal*, (2002). **31**: pp. 73–80.
96. Balinov, B., O. Söderman, and J.C. Ravey, Diffraction-like effects observed in the PGSE experiment when applied to a highly concentrated water/oil emulsion. *Journal of Physical Chemistry*, (1994). **98**(2): pp. 393–395.
97. Söderman, O. and U. Olsson, Dynamics of amphiphilic systems studied using NMR relaxation and pulsed field gradient experiments. *Current Opinion in Colloid & Interface Science*, (1997). **2**(2): pp. 131–136.
98. Giustini, M., G. Palazzo, A. Ceglie, J. Eastoe, A. Bumujdad, and R.K. Heenan, Studies of cationic and nonionic surfactant mixed microemulsions by small-angle neutron scattering and pulsed field gradient NMR. *Progress in Colloid and Polymer Science*, (2000). **115**: pp. 25–30.
99. Söderman, O. and M. Nydén, NMR in microemulsions. NMR translational diffusion studies of a model microemulsion. *Colloids and Surfaces a – Physicochemical and Engineering Aspects*, (1999). **158**(1–2): pp. 273–280.
100. Wennerström, H., O. Söderman, U. Olsson, and B. Lindman, Macroemulsions versus microemulsions. *Colloids and Surfaces A – Physicochemical and Engineering Aspects*, (1997). **123**: pp. 13–26.
101. Thiebaud, M., E.M. Dumay, and J.C. Cheffel, Pressure-shift freezing of o/w emulsions: influence of fructose and sodium alginate on undercooling, nucleation, freezing kinetics and ice crystal size distribution. *Food Hydrocolloids*, (2002). **16**: pp. 527–545.
102. Flores, A.A. and H.D. Goff, Ice crystal size distributions in dynamically frozen model solutions and ice cream as affected by stabilizers. *Journal of Dairy Science*, (1999). **82**(7): pp. 1399–1407.